Research Square

Preprints are preliminary reports that have not undergone peer review.
They should not be considered conclusive, used to inform clinical practice,
or referenced by the media as validated information.

Anti-adhesive profile and peritoneal integration of a dynamic scaffold-coupled intraperitoneal shield in a porcine hernia model

Giuseppe Amato

amatomed@gmail.com

University of Palermo – Italy

Vito Rodolico

University of Palermo

Antonino Agrusa

University of Palermo

Roberto Puleio

IZSS

Giuseppe Di Buono

University of Palermo

Giovanni Cassata

CEMERIT- IZSS

Luca Cicero

CEMERIT- IZSS

Giorgio Romano

University of Palermo

Ilaria Terrana

University of Palermo

Giorgio Romano

University of Palermo

Article

Keywords: abdominal wall hernia, dynamic scaffold, foreign-body reaction, intraperitoneal adhesions, laparoscopy, tissue response

Posted Date: November 25th, 2026

DOI: https://doi.org/10.21203/rs.3.rs-11303300/v1

License: This work is licensed under a Creative Commons Attribution 4.0 International License.
Read Full License

Additional Declarations: Competing interest reported. Giuseppe Amato is the inventor, developer and patent owner of the S&S Hernia System evaluated in this study. The other authors declare no competing interests.

Anti-adhesive profile and peritoneal integration of a dynamic scaffold-coupled intraperitoneal shield in a porcine hernia model.

Giuseppe Amato[1], Vito Rodolico[2], Antonino Agrusa[1], Roberto Puleio[3], Giuseppe Di Buono[1], Giovanni Cassata[4], Luca Cicero[4], Giorgio Romano[5], Ilaria Terrana[5], Giorgio Romano[1]

1) Department of precision medicine in medical, surgical and critical areas. University of Palermo - Italy
2) Department PROMISE, Section Pathological Anatomy University of Palermo - Italy
3) Department of Pathologic Anatomy and Histology, IZSS, Palermo - Italy
4) CEMERIT- IZSS, Palermo, Italy
5) Postgraduate School of General Surgery University of Palermo – Italy

Corresponding author

Prof. Giuseppe Amato MD FACS
Department of precision medicine in medical, surgical and critical areas. University of Palermo – Italy - Via del Vespro 129 - 90127 Palermo PA – Italy
e-mail: amatomed@gmail.com
Tel. +39 337963197
Fax +390916552836

Abstract

Background
Visceral adhesion formation remains an unresolved limitation of intraperitoneal prosthetic hernia repair. The S&S Hernia System (S&S) was developed to address this problem by coupling a defect-obliterating dynamic regenerative scaffold to a reticulated intraperitoneal shield, thereby transmitting cyclical abdominal wall motion from the scaffold to the shield. This study evaluated the temporal behavior of visceral adhesions and characterized the shield–peritoneal interface histologically.

Methods
Twenty S&S devices were implanted laparoscopically into bilateral abdominal-wall defects in 10 female pigs and assessed at 1, 3–4, or 5–8 months. Serial laparoscopy evaluated shield coverage and adhesions. Haematoxylin and eosin and Azan–Mallory-stained specimens were examined for inflammatory infiltrates, foreign-body reaction, fibrotic encapsulation and tissue organization.

Results
At 1 month, 2 of 20 shields (10%) had thin adhesion bands; neither was detectable at 3 months. No visceral adhesion involved any shield at explantation. Shield surfaces developed smooth, continuous tissue coverage integrated with the parietal peritoneum. Vascularized collagenous tissue extended through the shield, with a continuous flattened surface lining at 4 months. No morphologically detectable device-associated inflammatory cellular infiltrate was identified in examined sections from 1 month onwards; foreign-body giant cells, granulomatous inflammation and dense fibrotic encapsulation were absent.

Conclusion
The disappearance of the two early-bands and absence of adhesions on all shields at explantation demonstrated an anti-adhesive profile. Structural integration with the parietal peritoneum without a detectable established inflammatory foreign-body response provided biological context. Dynamic scaffold-to-shield motion is a plausible contributing mechanism that warrants controlled testing as a potentially durable anti-adhesive strategy.

Keywords: abdominal wall hernia; dynamic scaffold; foreign-body reaction; intraperitoneal adhesions; laparoscopy; tissue response

Introduction

Intraperitoneal mesh repair places permanent prosthetic material adjacent to the abdominal viscera. Implantation may induce macrophage recruitment, foreign-body giant-cell formation, collagen deposition and fibrotic encapsulation [1,2]. At the peritoneal interface, inflammation and impaired fibrinolysis may permit transient fibrinous bridges to undergo fibrovascular organization and become mature adhesions [3,4]. Conventional flat meshes address this risk principally through absorbable or permanent surface barriers. Although these barriers may reduce early adhesions, their protection may diminish with degradation, and experimental histology and clinical reoperations show that inflammation, fibrosis and visceral attachment are not consistently eliminated [5–11]. Adhesion prevention therefore remains an unresolved limitation of passive intraperitoneal prostheses.

Dynamic regenerative scaffolds (DRSs) were developed according to a different biological and mechanical principle. A compliant three-dimensional scaffold occupies the defect and deforms with cyclical abdominal-wall loading rather than functioning as planar reinforcement. Experimental and human studies of ProFlor, the first-generation DRS, demonstrated vascularized tissue ingrowth with newly formed skeletal muscle fibres, arteries, veins and neural elements, accompanied by angiogenic, myogenic and neurotrophic markers [12–15]. Concordance between human magnetic resonance imaging and porcine histology further supported an association between mechanical responsiveness and regenerative tissue development [16].

The S&S Hernia System extends this principle to laparoscopic intraperitoneal repair by mechanically coupling a defect-obliterating scaffold to a permanent 1.2-mm-thick reticulated shield. Cyclical scaffold deformation is thereby transmitted to the shield and its margins. Previous porcine studies documented vascular, muscular and neural development within the scaffold [17]. In 20 implanted devices, two thin adhesion bands involving the shield at 1 month were no longer detectable at 3 months, and no visceral adhesions were present at explantation [18]. However, the shield-specific tissue response underlying this behaviour was not the primary focus of that investigation.

The present secondary analysis therefore primarily examined the temporal behavior of visceral adhesions to the intraperitoneal shield by serial laparoscopy and explantation assessment from 1 to 8 months. Histological examination was undertaken to characterize the shield–peritoneal interface and identify tissue features potentially associated with the observed adhesion behavior, including morphologically detectable device-associated inflammatory cellular infiltrates, foreign-body giant cells, granulomatous inflammation, fibrotic encapsulation, collagen organization, vascularized tissue ingrowth, surface coverage and structural integration with the parietal peritoneum. Scaffold findings were reported descriptively only to provide biological context for the mechanically coupled system.

Methods

Study design, ethical approval and animal source.

This secondary, component-focused analysis used serial laparoscopic observations and archived specimens from the previously reported porcine study of the S&S Hernia System [18]. No additional animals or procedures were used. Reporting followed ARRIVE 2.0 [19].

The original animal experiment was conducted between February 2022 and November 2024 at the Istituto Zooprofilattico Sperimentale della Sicilia, Italy. The experimental protocol was reviewed by the Institute's Animal Welfare Body (Organismo Preposto al Benessere degli Animali, OPBA), which issued a favourable opinion, and was subsequently authorized by the Italian Ministry of Health (Authorization No. 379/2021-PR; protocol reference 28875.36). All procedures were carried out in accordance with the approved protocol and applicable guidelines and regulations, including Italian Legislative Decree No. 26 of 4 March 2014, implementing Directive 2010/63/EU. Reporting followed the ARRIVE 2.0 guidelines [19].

The pigs were obtained from Azienda Agricola Randazzo, C/da Pietralunga, Monreale (PA) - Italy, the supplying establishment identified in the authorized research project. Animal provenance and health status were documented through the accompanying veterinary health and traceability records.

Ten female pigs aged 4–6 months and weighing 40–60 kg constituted the study cohort. Sex was not an experimental variable, and no between-sex comparison was planned. Two lower abdominal-wall muscular defects were created in each animal, and one device was implanted per defect, yielding 20 devices and shields. The sample size and assessment intervals were predetermined in the original protocol; no additional sample-size calculation was performed for this qualitative secondary analysis. There was no comparator prosthesis.

Anaesthesia, perioperative management and euthanasia

Premedication comprised tiletamine–zolazepam (6.3 mg/kg) and xylazine (2.3 mg/kg). General anaesthesia was induced with propofol (0.5 mg/kg) and maintained with isoflurane; pancuronium (0.07 mg/kg) was administered for neuromuscular blockade. Oxytetracycline (20 mg/kg daily) was administered postoperatively for 3 days. Additional perioperative details are reported elsewhere [18].

The nine animals that reached their scheduled endpoints were euthanized under general anaesthesia using Tanax (5 mL per 35 kg body weight), administered by intravenous injection. Euthanasia was performed by appropriately qualified personnel in accordance with the protocol authorized by the Italian Ministry of Health. One animal died at 4 weeks before its scheduled endpoint; the circumstances and inclusion of its specimens are described in the Results.

Device and implantation

The injection-moulded device comprised an eight-rayed polypropylene-based thermoplastic-elastomer (TPE) structure constrained around a central mast and a 10 × 8 cm, 1.2-mm-thick reticulated shield (Fig. 1A). During delivery, the constrained cylindrical structure was termed the *stent*. Passage of the shield beyond the mast stops released it into an approximately 4.5-cm-diameter three-dimensional scaffold mechanically coupled to the shield (Fig. 1B).

Two approximately 3.5-cm defects were created bilaterally by electrocautery. Each device was introduced through a 12-mm trocar, positioned within a defect and deployed. The scaffold occupied the defect while the shield unfolded against the intraperitoneal surface and faced the viscera (Fig. 1C). No peritoneal flap, further dissection, sutures, tacks, adhesives or other fixation were used. The redundant mast was excised. Ultrasonography assessed scaffold position and tissue development (Fig. 1D).

Follow-up and sampling

Two animals (four devices) were assessed at 1 month, three (six devices) at 3–4 months and five (ten devices) at 5–8 months. Scheduled ultrasonography and laparoscopy assessed device position, shield coverage and the presence, location and persistence of visceral attachments. At the endpoint, final laparoscopy was undertaken under general anesthesia, followed by euthanasia according to the approved protocol, laparotomy and en bloc implant removal. Scaffold and shield-interface tissues were sampled separately.

Histological assessment

Specimens were fixed for at least 12 h in 10 per cent neutral phosphate-buffered formalin and embedded in paraffin. Both devices from each animal were sampled separately. Because block selection depended on explant geometry and tissue availability, a fixed number of blocks per device had not been prescribed. This analysis included all archived blocks containing an identifiable scaffold–tissue or shield–tissue interface with sufficient adjacent tissue for assessment. Sections without an interpretable implant interface were not used to attribute findings to the device.

Serial 4-μm sections were stained with hematoxylin and eosin. Additional available sections underwent Azan–Mallory staining (Bio-Optica, Milan, Italy) to assess collagen, connective-tissue organization, skeletal muscle, vascular structures and reticulated-shield ingrowth. Sections were examined by bright-field microscopy (Leica DMLB); images were acquired using a Nikon DS-Fi-1 camera and NIS Basic Research software.

Two pathologists examined coded sections while blinded to postoperative interval. Shield and scaffold interfaces were assessed separately. Shield assessment addressed morphologically detectable device-associated inflammatory cellular infiltrates, foreign-body giant cells, granulomatous inflammation, dense fibrotic encapsulation, vascularized tissue ingrowth, collagen organization, continuity of the visceral surface lining and structural integration with the parietal peritoneum. Assessment was qualitative; no inflammatory grading or immunophenotyping was performed. Inflammation was attributed to the device only when spatially contiguous with the material or centred on the interface. Unrelated cellular foci were classified as non-specific. Scaffold specimens were assessed descriptively to provide biological context.

Outcomes and analysis

The principal outcome was the temporal presence or absence of visceral adhesions involving the shield, assessed by serial laparoscopy and at explantation. Secondary outcomes were macroscopic shield coverage and shield histomorphology, including device-associated inflammatory cellular infiltrates, foreign-body reaction, fibrotic encapsulation, collagenous and vascular integration, surface-lining continuity and structural integration with the parietal peritoneum. Scaffold organization was descriptive. The animal was the biological unit; its two devices were paired observational units and were not treated as independent replicates. Results were summarized descriptively by interval and component as absolute numbers, with percentages where informative. No inferential comparisons were performed

Results

Animal and device outcomes

All 20 S&S devices were fully deployed and remained in their intended positions without migration or macroscopic shrinkage. One animal assigned to the 1-month group died at 4 weeks from

intestinal obstruction caused by faecal impaction. Necropsy showed both devices retained without displacement or visceral adhesions; these specimens were included in the 1-month assessment. The remaining nine animals reached their planned endpoints, and all devices were available for evaluation. The constrained delivery configuration and expanded scaffold–shield arrangement are illustrated in Fig. 1A,B. Laparoscopy confirmed bilateral defect coverage by the deployed shields facing the abdominal viscera (Fig. 1C). Ultrasonography showed preservation of the three-dimensional scaffold configuration and tissue development within its internal spaces, illustrated at 6 months in Fig. 1D.

Adhesion behavior

At the 1-month laparoscopic assessment, 2 of 20 shields (10%) displayed a thin adhesion band, whereas 18 (90%) were adhesion-free. The illustrated band connected a bowel loop to the left shield (Fig. 2A). At repeat laparoscopy in the same animal at 3 months, this attachment was no longer detectable, with no residual bridge or adherent bowel at the previously involved site (Fig. 2B). The second early band followed the same temporal course [18]. Neither band underwent adhesiolysis. No visceral adhesions were detected at subsequent laparoscopic assessments from 3 months onward, and none was present on any of the 20 shields in the 10 animals at explantation.

Serial observations also documented changes in the contour of the tissue covering the shields. At 1 month, the right shield in Fig. 2A exhibited prominent tissue folds with an irregular contour. By 3 months, this covering appeared less exuberant, more closely apposed to the underlying implant and more regular in outline (Fig. 2B). In a further serial comparison, the left shield showed a smooth contour at 3 months, whereas small tissue projections arose from the right shield without visible attachment to the abdominal viscera (Fig. 3A). At 6 months in the same animal, these projections were no longer visible; the right shield showed a more regular contour and a vascularized covering continuous with the surrounding parietal peritoneum (Fig. 3B). These unattached projections were distinct from the bowel-to-shield adhesion band documented in Fig. 2A.

Additional laparoscopic views immediately before explantation showed bilateral tissue coverage continuous with the parietal peritoneum at 3 months (Fig. 4A) and a smooth covering with visible superficial vessels at 4 months (Fig. 4B). At 6 months, both shields were covered by confluent tissue following the implant contours, without visible adherent bowel or adhesion bands (Fig. 5A,B). The vesical ligament visible between or in front of the shields was identified as an anatomical structure rather than an adhesion.

At 8 months, the reticulated contours remained identifiable beneath the tissue covering, and no visceral adhesions were visible (Fig. 6A). The medial portions of the two shields remained overlapping, preserving the relative configuration recorded immediately after deployment in the same animal (Fig. 6B). This comparison documented maintenance of their relative positioning.

Macroscopic findings after explantation

All explanted devices inspected and bisected through the scaffold showed viable newly formed tissue filling its three-dimensional structure. The associated shield surface was smooth and uniform, without adherent visceral tissue or organized adhesion bands (Fig. 7A). Representative explanted shields showed vascularized tissue distributed through the reticulated structure at 1 month (Fig. 7B), more uniformly organized tissue coverage at 3 months (Fig. 7C), and a smooth, uniformly distributed covering at 6 months (Fig. 7D). No adherent visceral tissue or adhesion bands were visible on these specimens, and no macroscopic fibrotic thickening was observed.

Histological findings at the shield interface

At the earliest scheduled histological assessment, 1 month after implantation, no morphologically detectable device-associated inflammatory cellular infiltrate was identified in the examined shield-associated sections. Multinucleated foreign-body giant cells, granulomatous inflammation and dense fibrotic encapsulation were also absent. Vascularized connective tissue extended through the reticulated shield and surrounded its material profiles (Fig. 8A). Organized connective tissue immediately adjacent to the shield contained a prominent elongated, thin-walled venous structure (Fig. 8B). Additional fields showed connective tissue surrounding multiple shield profiles without fibrotic isolation (Fig. 8C) and multiple patent vascular structures within tissue directly contacting the implant (Fig. 8D).

At 4 months, connective tissue extended through the shield structure and surrounded its profiles. A continuous flattened surface lining covered a developed connective-tissue layer along the visceral aspect (Fig. 9A). Mature connective tissue containing small vascular structures surrounded the shield in an additional field (Fig. 9B), while organized tissue containing skeletal muscle bundles and developed vascular structures was present in the 4-month shield biopsy illustrated in Fig. 9C. No morphologically detectable device-associated inflammatory cellular infiltrate was identified in these sections.

At 6 months, low-power examination showed a smooth tissue contour and mature connective-tissue architecture adjacent to the shield (Fig. 9D). Higher-magnification examination demonstrated organized, vascularized fibrocollagenous tissue directly contacting the shield, with adjacent loose connective tissue containing small-calibre vascular structures (Fig. 10A). At 8 months, regenerated skeletal muscle bundles were continuous with organized connective tissue containing a developed thick-walled vascular structure extending towards the shield profile (Fig. 10B). Further sections showed skeletal muscle continuous with vascularized fibroadipose tissue containing a developed arterial structure (Fig. 10C), and muscle bundles associated with connective tissue containing multiple developed vascular structures adjacent to the implant (Fig. 10D). No morphologically detectable device-associated inflammatory cellular infiltrate, multinucleated foreign-body giant-cell reaction, granulomatous inflammation or dense fibrotic encapsulation was identified in the examined intermediate- or long-term sections.

Collagen organization at the shield interface

Azan–Mallory staining showed collagen distributed within the incorporated tissue rather than forming a dense circumferential capsule. At 1 month, blue-stained collagen-rich connective tissue extended throughout the tissue surrounding the shield profiles (Fig. 11A). At 4 months, collagenous tissue adjacent to the shield extended continuously between red-stained regenerated skeletal muscle bundles and beneath the continuous flattened lining of the visceral surface (Fig. 11B). At 8 months, mature collagen extended between muscle bundles and around developed vascular structures adjacent to the shield (Fig. 11C). A further section showed collagenous tissue following the shield contours and remaining continuous with the connective septa between skeletal muscle bundles (Fig. 11D). No discrete separating fibrotic capsule, morphologically detectable device-associated inflammatory cellular infiltrate or granulomatous foreign-body reaction was identified in all sections.

Descriptive scaffold findings

Scaffold histology provided biological context for the mechanically coupled scaffold–shield system. At 1 month, numerous newly formed small-calibre vessels were distributed within vascularized connective tissue directly contacting the scaffold material (Fig. 12A). At 3 months, organized tissue contained thick-walled arterial and thin-walled venous profiles together with newly developed skeletal muscle bundles (Fig. 12B). At 6 months, multiple developed arterial structures and a mature thin-walled venous structure were embedded in organized connective tissue adjacent to the scaffold (Fig. 12C). At 8 months, a developed thick-walled artery was surrounded by smaller vascular structures, connective tissue and skeletal muscle bundles (Fig. 12D). No morphologically detectable device-associated inflammatory cellular infiltrate, foreign-body giant-cell reaction, granulomatous inflammation or dense fibrotic encapsulation was identified in the examined scaffold sections.

Discussion

The principal finding of this study was the absence of visceral adhesions involving any of the 20 intraperitoneal shields at explantation. The only adhesions observed during follow-up were two thin bands at 1 month, neither of which remained detectable at 3 months and neither of which had undergone adhesiolysis. Serial laparoscopy therefore documented that these early bowel-to-shield attachments did not progress into persistent adhesions. Serial laparoscopic images also documented decreasing prominence or disappearance of unattached tissue projections during follow-up, alongside maintained shield positioning and peritoneal integration (Figs. 2–6). Histological examination provided biological context for this macroscopic outcome: the shield was structurally integrated with the parietal peritoneum through vascularized, collagen-containing tissue, while no morphologically detectable device-associated inflammatory cellular infiltrate was identified in the examined sections from the earliest scheduled assessment at 1 month. Foreign-body giant cells, granulomatous inflammation and dense fibrotic encapsulation were also absent.

This hierarchy is important. The adhesion findings were direct serial laparoscopic and explantation observations and constitute the primary outcome of the analysis. Histology cannot by itself demonstrate anti-adhesive efficacy or establish the mechanism responsible for the disappearance of the two bands. It can, however, show whether the shield–peritoneal interface exhibited the persistent inflammatory and fibrotic conditions that would be expected to support organization of transient fibrinous contacts into stable fibrovascular adhesions.

Conventional intraperitoneal prostheses approach adhesion prevention mainly through passive separation of the permanent mesh from the viscera. Experimental work has shown that protection from some absorbable coatings may diminish during degradation and phagocytosis [20], while systematic appraisal indicates that barrier materials reduce but do not eliminate adhesions [23]. Animal studies describe material-dependent inflammatory responses, perifilamentary fibrosis and visceral attachment [24,25]. Clinical reoperations after intraperitoneal mesh placement likewise document bowel or omental adhesions and increased technical difficulty during subsequent abdominal surgery [21,22, 27–30]. These findings show that an early physicochemical barrier does not necessarily determine the later biological and mechanical interface.

The S&S shield differs conceptually because it is a permanent reticulated structure mechanically coupled to a dynamically compliant scaffold rather than a flat mesh protected by a temporary

coating. In this series, the shield did not remain exposed or become isolated within a dense capsule. Progressive tissue coverage extended through its reticulation and became structurally continuous with the parietal peritoneum. This organization was accompanied by the absence of adherent viscera at explantation, rather than by replacement of one separating barrier with another.

The inflammatory findings offer one biologically coherent explanation for the observed adhesion behavior. Postoperative adhesions originate when fibrinous bridges between injured or persistently apposed peritoneal surfaces escape fibrinolysis and undergo fibroblast invasion, angiogenesis and collagen organization [3]. Mature human adhesions are cellular, vascularized, innervated and collagenous structures, consistent with an active reparative process rather than inert scar tissue [26]. An established inflammatory stimulus at an implant interface may sustain this progression. In the present specimens, however, no device-associated inflammatory cellular infiltrate was detectable from 1 month onwards, and no giant-cell, granulomatous or dense encapsulating response accompanied tissue incorporation of the shield.

This observation must be interpreted precisely. The first histological specimens were obtained at 1 month; an acute postoperative inflammatory phase before that time cannot be excluded. Evaluation was qualitative and did not include inflammatory cell counts, grading or immunophenotyping. The supported conclusion is therefore not that inflammation never occurred, but that no morphologically detectable device-associated inflammatory cellular infiltrate or established chronic foreign-body response was present in the examined shield sections at 1 month or later. This interval includes the period during which persistent fibrinous attachments would be expected to undergo fibrovascular organization.

The morphology of the shield interface provided further context. Vascularized connective tissue already extended through the reticulated structure at 1 month. At 4 months, a continuous flattened surface lining covered an organized subperitoneal connective-tissue layer, and the incorporated tissue was structurally continuous with the surrounding parietal peritoneum. Macroscopically, shield coverage became progressively smoother and more uniform. These observations document surface coverage and parietal-peritoneal integration; they are not used here to assign a specific cellular phenotype to the lining.

Serial observation strengthens the adhesion finding. Endpoint-only animal studies cannot determine whether an attachment formed earlier, enlarged or resolved. Here, the two bands were identified at 1 month and were subsequently absent without surgical separation. Their histological organization could not be examined after disappearance, but their temporal course argues against maturation into stable fibrovascular adhesions. The finding does not exclude brief or intermittent visceral contacts between examinations; it demonstrates that the observed early bands did not become persistent bowel-to-shield attachments. The paired views in Fig. 2A,B provide direct documentation of this change in the same animal.

The serial images additionally document evolution of the shield covering itself. In Fig. 2, the prominent, irregular folds over the right shield at 1 month were less exuberant and more closely apposed to the implant at 3 months. In a separate paired comparison, the small projections arising from the right shield at 3 months showed no visible connection to the viscera and were no longer visible at 6 months (Fig. 3A,B). These projections should therefore be distinguished from the bowel-to-shield band in Fig. 2A. Their presence did not, in itself, represent a visceral adhesion, and their subsequent disappearance was accompanied by a more regular tissue contour rather than a persistent attachment to adjacent bowel.

This distinction adds to the interpretation of the anti-adhesive profile: an initially exuberant surface covering did not necessarily persist or develop a visible visceral connection. The serial changes are consistent with remodelling of shield-associated tissue towards a smoother peritoneal surface.

Additional pre-explantation views document tissue coverage continuous with the parietal peritoneum and no visible visceral adhesions at 3 and 4 months (Fig. 4A,B) and at 6 months (Fig. 5A,B). These views complement the within-animal comparisons by showing the appearance of the interface across postoperative intervals. At 8 months, the medial overlap of the two shields remained identifiable (Fig. 6A), preserving the relative arrangement recorded at implantation (Fig. 6B). This supports maintained relative positioning while tissue incorporation developed. Tissue integration and the absence of visible visceral attachments were thus observed even in this overlapping configuration.

Azan–Mallory staining was consistent with integration rather than fibrotic isolation. Collagen was distributed throughout shield-associated tissue, around vessels and between regenerated skeletal muscle bundles. It did not form a dense circumferential layer separating the material from adjacent structures. Collagen deposition is expected during repair, whereas concentric collagen accumulation associated with continuing macrophage and giant-cell activity characterizes foreign-body encapsulation. The architecture observed here therefore provides a plausible tissue basis for stable incorporation without creating a rigid isolating interface.

Material compatibility probably contributed to this response, but the present design cannot separate polymer composition from reticulated geometry, three-dimensional architecture or mechanical behavior. The descriptive scaffold findings nevertheless provide relevant context. First-generation ProFlor DRS studies documented progressive development of skeletal muscle, arteries, veins and neural structures, together with angiogenic, myogenic and neurotrophic markers, in experimental and human specimens [12–16]. Comparable vascular, muscular and neural development was subsequently reported within the S&S scaffold [17, 18]. These observations distinguish DRS incorporation from non-specific fibrous filling and provide independent support for considering cyclical mechanical loading an active biological design variable. The collagen architecture in Fig. 11A–D complements the macroscopic evidence of peritoneal integration, showing collagen distributed within the incorporated tissue rather than forming a dense capsule separating the shield from the surrounding structures.

In the S&S configuration, abdominal-wall loading deforms the scaffold occupying the defect, and the mechanical connection transmits this movement to the shield and its peripheral margins. Supplementary Video 1 demonstrates this transmission qualitatively. Repetitive shield displacement could shorten the duration and stability of contact with adjacent viscera, thereby limiting persistence of immature fibrinous bridges before fibrovascular invasion and collagen maturation. The disappearance of the two early bands is compatible with this mechanism, while the organized, non-encapsulating peritoneal integration indicates that continued movement did not prevent tissue incorporation. The accompanying reduction in surface exuberance is consistent with ongoing tissue adaptation, to which dynamic scaffold-to-shield motion may contribute.

The present data cannot assign causality to motion alone. There was no static control, and shield displacement was not quantified in vivo. Moreover, no otherwise equivalent commercial shield exists in dynamically coupled and static forms; comparison with an unrelated prosthesis would confound motion with polymer, thickness, geometry and surface structure. A mechanistically appropriate experiment would compare shields identical in all respects except whether scaffold movement is transmitted to them, with predefined adhesion scoring and quantitative measurement of displacement and contact dynamics. Until then, dynamic scaffold-to-shield transmission remains

a plausible contributing mechanism, whereas disappearance of the early bands and absence of adhesions at explantation are observed outcomes.

The procedural characteristics may also be relevant. The device is introduced in a constrained configuration and expands rapidly into a self-retaining scaffold–shield arrangement. Defect occupation and visceral coverage require no peritoneal flap, preperitoneal dissection, sutures, transfascial fixation, tacks or adhesives. Limiting dissection and traumatic fixation may reduce bleeding, ischaemia, fibrin deposition and additional foreign-body stimuli. The system therefore combines limited implantation trauma, absence of a detectable established inflammatory infiltrate and continuing mechanical responsiveness of a shield structurally integrated with the parietal peritoneum. In this series, procedural simplification was not accompanied by migration, macroscopic shrinkage or loss of defect coverage.

The combination of serial observations appears distinctive: only two thin early adhesion bands among 20 shields, disappearance of both by 3 months without adhesiolysis, and no visceral adhesions at explantation, together with vascularized peritoneal integration, collagen incorporated within the organized tissue rather than forming an isolating capsule, and no morphologically detectable device-associated inflammatory cellular infiltrate in the examined sections.

An additional translational consideration concerns the quadrupedal posture of the porcine model. In pigs, the ventral abdominal wall constitutes the gravity-dependent surface of the abdominal cavity; the viscera may therefore remain in closer and more sustained apposition to a ventrally positioned intraperitoneal shield than in humans in the upright position, in whom the gravitational vector is directed predominantly caudally. The shield may consequently have been evaluated under a mechanically demanding visceral-contact environment. In this context, the disappearance of the two early adhesion bands and the absence of visceral adhesions from 3 months onward are particularly noteworthy and may be regarded as findings obtained under a conservative mechanical challenge. However, because visceral contact pressure and duration were not quantified and species-specific differences in peritoneal healing remain, the porcine model cannot formally be designated as a validated worst-case scenario.

This sustained opportunity for visceral contact also strengthens the biological plausibility of the proposed dynamic mechanism: the absence of mature adhesions cannot readily be attributed to insufficient exposure of the shield to the viscera, whereas repeated scaffold-to-shield deformation may have limited the stabilization and organization of transient contacts. Taken together, these observations support an anti-adhesive profile of the system. They do not establish superiority over existing intraperitoneal prostheses, which would require prospective head-to-head comparison using standardized macroscopic and histological outcomes.

Several limitations require emphasis. This was a secondary analysis of a small, uncontrolled preclinical series. Two shields were implanted in each animal and were paired observations rather than independent biological replicates. Assessment was qualitative, and the earliest specimens were obtained at 1 month, precluding evaluation of the acute inflammatory phase. Resolved adhesion bands could not be sampled, and cytokine activity, fibrinolysis, shield displacement and visceral contact dynamics were not measured.

Despite these limitations, the macroscopic finding is clear: the two thin adhesion bands observed at 1 month were no longer detectable at 3 months, and none of the 20 shields had a visceral adhesion at explantation. Histology supplied a coherent biological context by demonstrating vascularized structural integration with the parietal peritoneum, organized collagen deposition and no

morphologically detectable device-associated inflammatory cellular infiltrate or dense fibrotic encapsulation from 1 month onwards.

The S&S shield therefore exhibited an anti-adhesive profile while becoming structurally integrated with the parietal peritoneum. Controlled studies are required to determine the relative contributions of dynamic scaffold-to-shield motion, device architecture, material and atraumatic fixation-free and dissection-free implantation to this outcome.

References

1. Klinge U, Klosterhalfen B, Müller M, Schumpelick V. Foreign body reaction to meshes used for the repair of abdominal wall hernias. Eur J Surg. 1999;165:665–673. doi:10.1080/11024159950189726.
2. Heymann F, von Trotha KT, Preisinger C, Lynen-Jansen P, Roeth AA, Geiger M, et al. Polypropylene mesh implantation for hernia repair causes myeloid cell-driven persistent inflammation. JCI Insight. 2019;4:e123862. doi:10.1172/jci.insight.123862.
3. Arung W, Meurisse M, Detry O. Pathophysiology and prevention of postoperative peritoneal adhesions. World J Gastroenterol. 2011;17:4545–4553. doi:10.3748/wjg.v17.i41.4545.
4. Matthews BD, Pratt BL, Pollinger HS, Backus CL, Kercher KW, Sing RF, et al. Assessment of adhesion formation to intra-abdominal polypropylene mesh and polytetrafluoroethylene mesh. J Surg Res. 2003;114:126–132. doi:10.1016/S0022-4804(03)00158-6.
5. Schreinemacher MHF, van Barneveld KWY, Peeters E, Miserez M, Gijbels MJJ, Greve JWM, et al. Coated meshes for hernia repair provide comparable intraperitoneal adhesion prevention. Surg Endosc. 2013;27:4202–4209. doi:10.1007/s00464-013-3021-5.
6. Fuziy RA, Artigiani Neto R, Caetano Junior EM, Alves AKS, Lopes Filho GJ, Linhares MM. Comparative study of four different types of intraperitoneal mesh prostheses in rats. Acta Cir Bras. 2019;34:e201900703. doi:10.1590/S0102-865020190070000003.
7. Raptis DA, Vichova B, Breza J, Skipworth J, Barker S. A comparison of woven versus nonwoven polypropylene and expanded versus condensed polytetrafluoroethylene on their intraperitoneal incorporation and adhesion formation. J Surg Res. 2011;169:1–6. doi:10.1016/j.jss.2009.12.014.
8. Takács I, Horváth S, Molnár A, et al. Comparative immunohistochemical study of tissue integration of macroporous and laminar surgical meshes. Histol Histopathol. 2011;26:821–830. doi:10.14670/HH-26.821.
9. Halm JA, de Wall LL, Steyerberg EW, Jeekel J, Lange JF. Intraperitoneal polypropylene mesh hernia repair complicates subsequent abdominal surgery. World J Surg. 2007;31:423–429. doi:10.1007/s00268-006-0317-9.
10. Fortelny RH, Petter-Puchner AH, Glaser KS, Offner F, Benesch T, Rohr M. Adverse effects of polyvinylidene fluoride-coated polypropylene mesh used for laparoscopic intraperitoneal onlay repair of incisional hernia. Br J Surg. 2010;97:1140–1145. doi:10.1002/bjs.7082.
11. Chelala E, Debardemaeker Y, Elias B, Charara F, Dessily M, Allé JL. Eighty-five redo surgeries after 733 laparoscopic treatments for ventral and incisional hernia: adhesion and recurrence analysis. Hernia. 2010;14:123–129. doi:10.1007/s10029-010-0637-4.
12. Amato G, Romano G, Puleio R, Agrusa A, Goetze T, Gulotta E, et al. Neomyogenesis in 3D dynamic responsive prosthesis for inguinal hernia repair. Artif Organs. 2018;42:1216–1223. doi:10.1111/aor.13286.

13. Amato G, Agrusa A, Puleio R, Calò PG, Goetze T, Romano G. Neo-nervegenesis in 3D dynamic responsive implant for inguinal hernia repair: qualitative study. Int J Surg. 2020;76:114–119. doi:10.1016/j.ijsu.2020.02.046.
14. Amato G, Puleio R, Rodolico V, Agrusa A, Calò PG, Di Buono G, et al. Enhanced angiogenesis in the 3D dynamic responsive implant for inguinal hernia repair ProFlor. Artif Organs. 2021;45:933–942. doi:10.1111/aor.13926.
15. Amato G, Puleio R, Romano G, Calò PG, Di Buono G, Cicero L, et al. Physiologic cyclical load on inguinal hernia scaffold ProFlor turns biological response into tissue regeneration. Biology (Basel). 2023;12:434. doi:10.3390/biology12030434.
16. Amato G, Agrusa A, Puleio R, Micci G, Cassata G, Cicero L, et al. A regenerative 3D scaffold for inguinal hernia repair: MR imaging and histological cross evidence. Qualitative study. Int J Surg. 2021;96:106170. doi:10.1016/j.ijsu.2021.106170.
17. Amato G, Agrusa A, Puleio R, Rodolico V, Cicero L, Cassata G, et al. Dynamic behavior of the Stenting & Shielding Hernia System fosters neomyogenesis in an experimental porcine model. Bioengineering (Basel). 2025;12:883. doi:10.3390/bioengineering12080883.
18. Amato G, Romano G, Cicero L, Cassata G, Di Buono G, Romano G, et al. The dynamic regenerative scaffold Stenting and Shielding Hernia System for dissection-free, atraumatic hernioplasty: results of an experimental animal study. Sci Rep. 2025;15:38277. doi:10.1038/s41598-025-24487-6.
19. Percie du Sert N, Hurst V, Ahluwalia A, Alam S, Avey MT, Baker M, et al. The ARRIVE guidelines 2.0: updated guidelines for reporting animal research. PLoS Biol. 2020;18:e3000410. doi:10.1371/journal.pbio.3000410.
20. Schreinemacher MHF, Emans PJ, Gijbels MJJ, Greve JWM, Beets GL, Bouvy ND. Degradation of mesh coatings and intraperitoneal adhesion formation in an experimental model. Br J Surg. 2009;96:305–313.
21. Jenkins ED, Yom V, Melman L, Brunt LM, Eagon JC, Frisella MM, et al. Prospective evaluation of adhesion characteristics to intraperitoneal mesh and adhesiolysis-related complications during laparoscopic re-exploration after prior ventral hernia repair. Surg Endosc. 2010;24:3002–3007.
22. Wassenaar EB, Schoenmaeckers EJP, Raymakers JTFJ, Rakic S. Subsequent abdominal surgery after laparoscopic ventral and incisional hernia repair with an expanded polytetrafluoroethylene mesh: a single institution experience with 72 reoperations. Hernia. 2010;14:137–142.
23. Waldron MG, Judge C, Farina L, O'Riordan JM. Barrier materials for prevention of surgical adhesions: systematic review. BJS Open. 2022;6:zrac075.
24. Moretti AIS, Rios EC, Soriano FG, de Souza HP, Abatepaulo F, Barbeiro DF, et al. Nitric oxide modulates metalloproteinase-2, collagen deposition and adhesion rate after polypropylene mesh implantation in the intra-abdominal wall. Acta Biomater. 2012;8:108–115.
25. Conze J, Junge K, Klinge U, Weiss C, Polivoda M, Oettinger AP, et al. Intraabdominal adhesion formation of polypropylene mesh: influence of coverage of omentum and polyglactin. Surg Endosc. 2005;19:798–803.
26. Herrick SE, Mutsaers SE, Ozua P, Sulaiman H, Omer A, Boulos P, et al. Human peritoneal adhesions are highly cellular, innervated, and vascularized. J Pathol. 2000;192:67–72.
27. Sharma A, Chowbey P, Kantharia NS, Baijal M, Soni V, Khullar R. Previously implanted intraperitoneal mesh increases morbidity during re-laparoscopy: a retrospective, case-matched cohort study. Hernia. 2018;22:343–351. doi:10.1007/s10029-017-1686-8.
28. Patel PP, Love MW, Ewing JA, Warren JA, Cobb WS, Carbonell AM. Risks of subsequent abdominal operations after laparoscopic ventral hernia repair. Surg Endosc. 2017;31:823–828. doi:10.1007/s00464-016-5038-z.

29. Turcu F, Arnăutu O, Copăescu C. Adhesiolysis-related challenges for laparoscopic procedures after ventral hernia repair with intraperitoneal mesh. Chirurgia (Bucur). 2019;114:39–47. doi:10.21614/chirurgia.114.1.39.
30. Delorme T, Cottenet J, Abo-Alhassan F, Bernard A, Ortega-Deballon P, Quantin C. Does intraperitoneal mesh increase the risk of bowel obstruction? A nationwide French analysis. Hernia. 2024;28:419–426. doi:10.1007/s10029-023-02885-x.

Acknowledgements

Author contributions

A G: Conceptualization
R V: Investigation, supervision
Agrusa A: Methodology
P R: Investigation,
D B G: Writing—review and editing
C G: Resources
C L: Data curation
R G: Writing original draft
T I: Review and editing
R G: Validation

Funding

This research received no external funding.

Conflict of interest

Giuseppe Amato is the inventor, developer and patent owner of the S&S Hernia System evaluated in this study. The other authors declare no competing interests.

Data availability

The datasets used and/or analysed during the current study available from the corresponding author on reasonable request.

Figures

Figure 1- A: S&S device before intraperitoneal insertion. The eight-rayed structure is constrained around the central mast in its cylindrical delivery configuration, while the reticulated shield is threaded onto the mast and remains free to slide during deployment. – B: Fully deployed device showing the expanded three-dimensional scaffold and the 10 × 8 cm, 1.2-mm-thick reticulated shield locked to the central mast. – C: Laparoscopic view of two S&S devices after bilateral implantation in the lower abdominal wall. The shields overlap the muscular defects and face the abdominal viscera. – D: Ultrasonographic image obtained 6 months after implantation. The scaffold is outlined by the red dotted circle, and the yellow arrows indicate tissue developed within its three-dimensional structure.

Figure 2. Serial laparoscopic disappearance of an early adhesion band and evolution of the tissue covering the S&S shields. (A) Laparoscopy 1 month after implantation shows a thin adhesion band connecting a bowel loop to the visceral surface of the left shield (yellow arrow). The tissue covering the right shield appears prominent, with an irregular, folded contour. The vesical ligament is identified as an anatomical landmark. (B) Repeat laparoscopy in the same animal at 3 months shows that the previously documented adhesion band is no longer detectable, with no residual bridge or

adherent bowel visible at the previously involved site. Compared with the 1-month appearance, the tissue covering the right shield appears less exuberant and more closely apposed to the underlying shield, with a more regular surface contour. The visible surfaces of both shields show continuous tissue coverage and macroscopic continuity with the surrounding parietal peritoneum. The vesical ligament is again identified to facilitate anatomical comparison.

Figure 3. Serial laparoscopic appearance of S&S shields at 3 and 6 months: resolution of tissue projections and peritoneal integration. (A) At 3 months after implantation, the left shield shows a smooth contour and macroscopic integration with the surrounding parietal peritoneum. Small tissue projections arise from the surface of the right shield (yellow arrows), without visible attachment to the abdominal viscera. (B) Repeat laparoscopy in the same animal at 6 months, immediately before euthanasia, shows that the previously observed projections are no longer visible. The right shield exhibits a more regular contour and a vascularized tissue covering continuous with the surrounding parietal peritoneum. Both shields remain identifiable beneath the tissue covering, with no visible adhesion bands connecting them to the abdominal viscera.

Figure 4. Laparoscopic appearance of S&S shields before explantation at 3 and 4 months: peritoneal integration and absence of visible visceral adhesions. (A) Laparoscopic assessment immediately before device explantation at 3 months shows both shields apposed to the abdominal wall, with tissue coverage continuous with the surrounding parietal peritoneum. The reticulated implant contours remain identifiable. No adhesion bands or adherent bowel are visible on either shield. (B) Laparoscopic assessment immediately before explantation at 4 months shows both shields incorporated into the parietal peritoneal surface. The tissue covering is smooth and continuous with the surrounding peritoneum, with visible superficial vessels. The underlying reticulated shield contours remain identifiable. No adhesion bands connect either shield to the abdominal viscera. The band-like structure in the foreground (yellow arrows) is the vesical ligament.

Figure 5. Laparoscopic appearance of S&S shields before explantation 6 months: peritoneal integration and absence of visible visceral adhesions. (A) Laparoscopic assessment of the shields immediately before explantation at 6 months shows both shields covered by a continuous tissue layer and macroscopically integrated with the surrounding parietal peritoneum. No visceral adhesion bands or adherent bowel are visible. The vesical ligament (yellow arrows) courses between the two devices (B) Laparoscopic assessment at 6 months, immediately before euthanasia, shows both shields incorporated into the parietal peritoneal surface, with a confluent tissue covering following the underlying implant contours. No visible adhesion bands connect either shield to the abdominal viscera.

Figure 6. Long-term laparoscopic appearance of S&S shields: peritoneal integration, maintained positioning, and absence of visible visceral adhesions. (A) Laparoscopic assessment of the S&S shields immediately before explantation at 8 months shows tissue coverage following the reticulated contours of both shields, without visible visceral adhesions. Their medial portions remain overlapping, preserving the relative configuration documented at implantation, consistent with maintained device positioning. The vesical ligament is indicated by yellow arrows. (B) Intraoperative view immediately after deployment in the same animal, documenting the initial overlap of the medial shield portions.

Figure 7. Macroscopic tissue integration within the S&S scaffold and progressive coverage of the visceral shield surface. (A) S&S Hernia System explanted 3 months after implantation and bisected to expose the three-dimensional scaffold, outlined by the red dotted line. Viable newly formed tissue fills the scaffold structure (yellow asterisks), whereas the reticulated shield is identified by black Xs. The shield surface is smooth and uniform, without adherent visceral tissue or organized

adhesion bands. (B) Visceral surface of a shield explanted 1 month after implantation. An early, well-vascularized covering tissue is already distributed throughout the reticulated shield structure. No adherent visceral tissue or adhesion bands are visible. (C) Visceral surface of a shield explanted 3 months after implantation. The tissue covering the shield appears more uniformly organized and integrated throughout the reticulated structure, without macroscopic fibrotic thickening, adherent visceral tissue, or adhesion bands. (D) Visceral surface of a shield explanted 6 months after implantation. A mature, smooth, and uniformly distributed tissue coverage integrated with the reticulated shield structure. No adherent visceral tissue or adhesion bands are present. At device explantation, no visceral adhesions were identified on any of the 20 shields implanted in the 10 animals.

Figure 8. Early tissue response at the S&S shield interface 1 month after implantation. (A) Low-power view showing vascularized connective tissue extending through the reticulated shield structure and surrounding the profiles of the shield material (black Xs). HE 25, (B) Higher-magnification view of organized connective tissue immediately adjacent to the shield profiles along the upper margin (black Xs). A prominent elongated, thin-walled venous structure is visible within the shield-associated tissue. HE 50x. (C) Additional low-power field showing vascularized connective tissue surrounding multiple shield profiles (black Xs), without fibrotic isolation of the implant. HE, 25x. (D) Higher-magnification view showing multiple patent vascular structures within the organized connective tissue in direct contact with the shield profile (black Xs). HE 50x. No morphologically detectable device-associated inflammatory cellular infiltrate, multinucleated foreign-body giant-cell reaction, granulomatous inflammation, or dense fibrotic encapsulation is present in any of the examined fields.

Figure 9 - A: Surface coverage and tissue integration of the S&S shield 4 months after implantation. Connective tissue extends through the reticulated shield structure and surrounds the profiles of the shield material (black Xs). Along the visceral aspect, the yellow asterisks identify a continuous, well-preserved flattened surface lining overlying a well-developed connective-tissue layer. No morphologically detectable device-associated inflammatory cellular infiltrate, multinucleated foreign-body giant-cell reaction, or granulomatous inflammation is identified within the newly formed tissue or at the shield–tissue interface. H&E, ×25. – B: Shield-associated tissue at 4 months post implantation. Mature connective tissue containing small vascular structures surrounds the shield profile visible along the lower margin (X). The tissue is completely free of inflammatory infiltration and granulomatous foreign-body reaction. HE 25x – C: Regenerative tissue within the S&S shield 4 months after implantation. Newly formed skeletal muscle bundles, organized connective tissue, and mature vascular structures occupy the scaffold, whose material profiles are identified by black Xs. The muscle fibers represent neomyogenesis occurring within the Dynamic Regenerative Scaffold and are not pre-existing abdominal-wall musculature. No inflammatory cellular infiltrate is present within the regenerated tissue or at the tissue–scaffold interface. HE 25x – D: Shield-associated tissue in a specimen excised 6 months post implantation. Low-power view showing a smooth tissue surface and mature connective-tissue architecture close to the shield structure (X). No inflammatory infiltrate is present. HE 25x

Figure 10 - A: Mature non-inflammatory tissue integration at the S&S shield interface 6 months after implantation. The profile of the shield material is identified by black Xs. The tissue in direct contact with the shield consists of mature, organized, and vascularized fibrocollagenous connective tissue. The yellow asterisks identify adjacent loose connective tissue containing small-caliber vascular structures. No inflammatory cellular infiltrate, multinucleated foreign-body giant-cell reaction, or granulomatous inflammation is present at the shield–tissue interface. HE 100x – B: Long-term regenerative tissue organization at the S&S shield interface 8 months after implantation. Mature regenerated skeletal muscle bundles are visible on the left. Organized connective tissue

containing a well-developed thick-walled vascular structure extends between the muscle and the profile of the shield material on the right (X). No inflammatory cellular infiltrate, multinucleated foreign-body giant-cell reaction, granulomatous inflammation, or dense fibrotic encapsulation is present at the shield–tissue interface. HE 25x – C: Long-term integration of the S&S shield with vascularized regenerative tissue 8 months after implantation. The profile of the shield material is identified by black Xs along the lower margin. Mature regenerated skeletal muscle on the left is continuous with organized fibroadipose connective tissue containing a well-developed thick-walled arterial structure. The tissue extends to and surrounds the shield profile without inflammatory cellular infiltrate, multinucleated foreign-body giant-cell reaction, granulomatous inflammation, or dense fibrotic encapsulation. HE 25x – D: Long-term non-inflammatory tissue organization at the S&S shield interface 8 months after implantation. The profile of the shield material is visible in the upper-right portion of the field (X). Mature regenerated skeletal muscle bundles occupy the left and lower regions and are continuous with organized connective tissue containing well-developed vascular structures. The tissue directly contacting the shield shows no inflammatory cellular infiltrate, multinucleated foreign-body giant-cell reaction, granulomatous inflammation, or dense fibrotic encapsulation. HE 50x

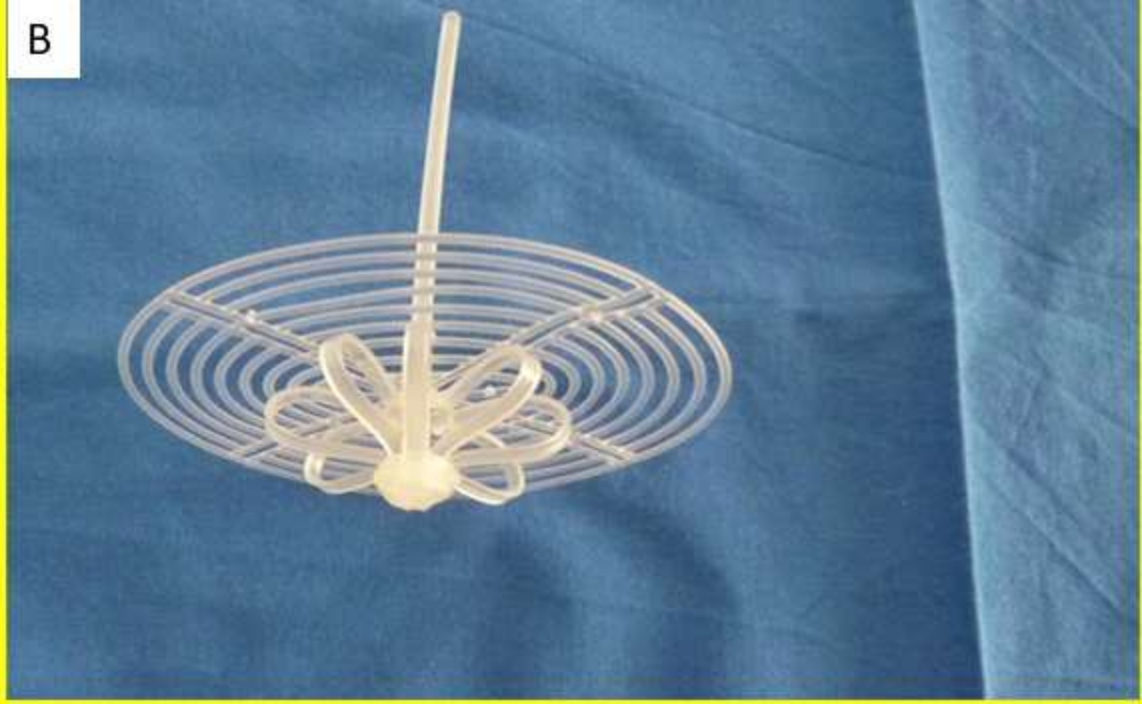
Figure 11 – A: Collagen organization at the S&S shield interface 1 month after implantation. Azan–Mallory staining shows collagen-rich connective tissue, stained blue, distributed throughout the tissue incorporated into the reticulated shield and surrounding the profiles of the shield material (X). The collagen is integrated within the newly formed tissue rather than arranged as a compact, concentric peri-implant capsule separating the shield from the surrounding tissue. AM 50x – (B) Collagen integration, regenerated skeletal muscle, and surface coverage at the S&S shield interface 4 months after implantation. Blue-stained collagenous connective tissue adjacent to the shield material profile (X) extends continuously into and between the red-stained regenerated skeletal muscle bundles, demonstrating structural integration of the shield-associated tissue. The collagen remains distributed within the incorporated tissue without forming a dense circumferential capsule separating the shield from the surrounding structures. On the right, the yellow asterisks identify a thin connective-tissue layer beneath a continuous flattened lining along the visceral surface. No morphologically detectable device-associated inflammatory cellular infiltrate or granulomatous foreign-body reaction is identified. AM 25x – C: Long-term collagen integration at the S&S shield interface 8 months after implantation. The profile of the reticulated shield material is identified by black Xs. Mature blue-stained collagenous tissue adjacent to the shield extends between the red-stained regenerated skeletal muscle bundles and surrounds mature vascular structures. The collagen remains integrated within the organized tissue architecture and does not form a discrete, dense, separating peri-implant capsule. AM 25x – D: Long-term collagen and skeletal muscle integration at the S&S shield interface 8 months after implantation. Azan–Mallory staining shows mature regenerated skeletal muscle bundles, stained red, surrounded and interconnected by organized collagenous connective tissue, stained blue. The collagen extends continuously to and closely follows the profiles of the shield material on the right (X), maintaining continuity with the connective septa between the muscle bundles. No inflammatory cellular infiltrate, granulomatous foreign-body reaction, or dense circumferential fibrotic capsule separates the shield from the surrounding regenerated tissue. AM 25x.

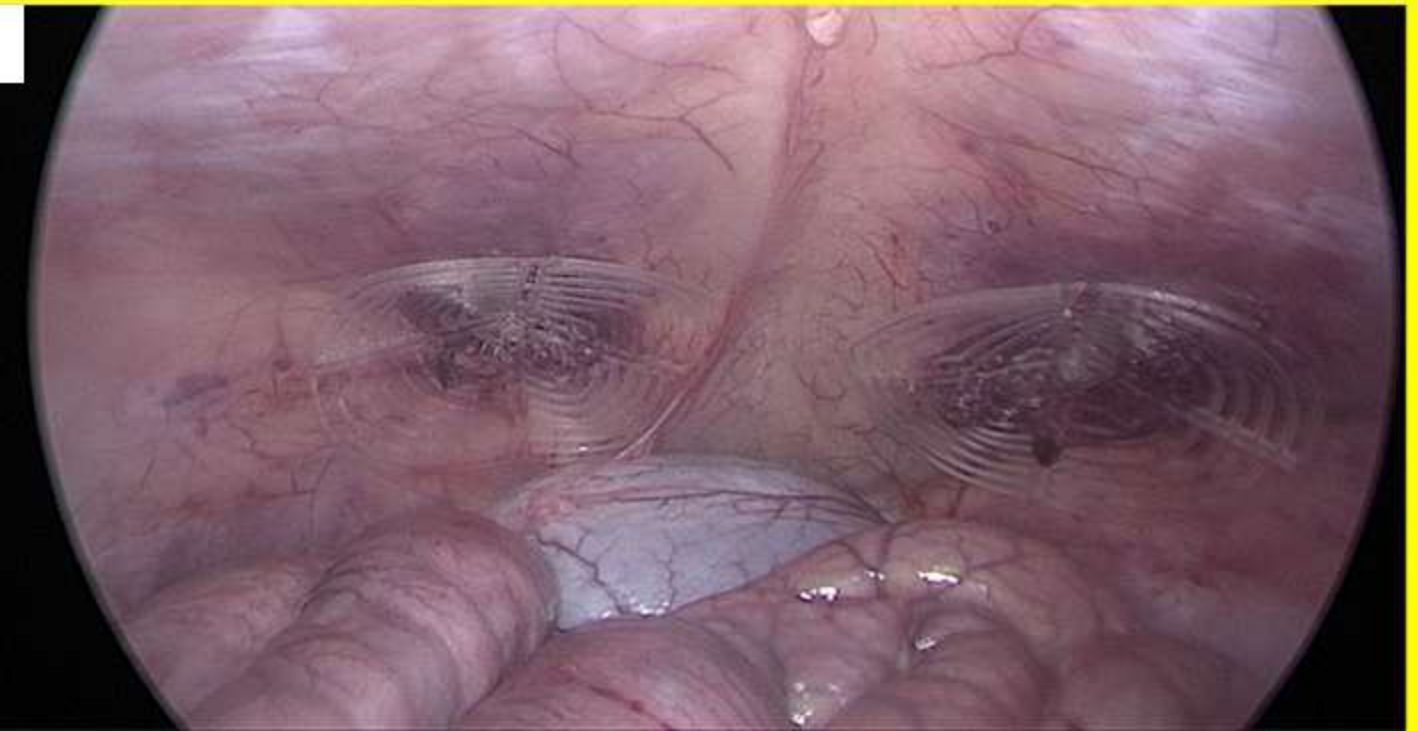
Figure 12 – A: Early non-inflammatory regenerative response within the S&S scaffold 1 month after implantation. Numerous newly formed small-caliber blood vessels (yellow asterisks) are distributed throughout well-vascularized connective tissue in direct contact with the scaffold material (X). No inflammatory cellular infiltrate is identifiable either within the tissue filling the scaffold or at the tissue–scaffold interface. No foreign-body giant-cell or granulomatous reaction is evident. HE 50X – B: Tissue maturation within the S&S scaffold at 3 months. Organized tissue contains vascular structures of different calibers, including thick-walled arterial profiles outlined by

the yellow dotted lines and thin-walled venous profiles indicated by the yellow asterisks. Newly developed skeletal muscle bundles are visible in the lower-right portion of the field. No inflammatory infiltrate is present around the scaffold material, identified by the X symbols. HE 50X. – C: Mature vascularized tissue within the S&S scaffold at 6 months. Multiple developed thick-walled arterial structures, indicated by the yellow asterisks, and a mature thin-walled venous structure, marked Y, are embedded in organized connective tissue adjacent to the scaffold material, identified by the black X symbols. The scaffold–tissue interface is free of inflammatory infiltration, foreign-body giant-cell reaction, and granulomatous inflammation. HE 100X. - D: Long-term regenerative tissue within the S&S scaffold at 8 months. A developed thick-walled artery, outlined by the yellow dotted line, is surrounded by smaller vascular structures, connective tissue, and newly developed skeletal muscle bundles. No inflammatory reaction surrounds the scaffold material, identified by the X. HE 50X

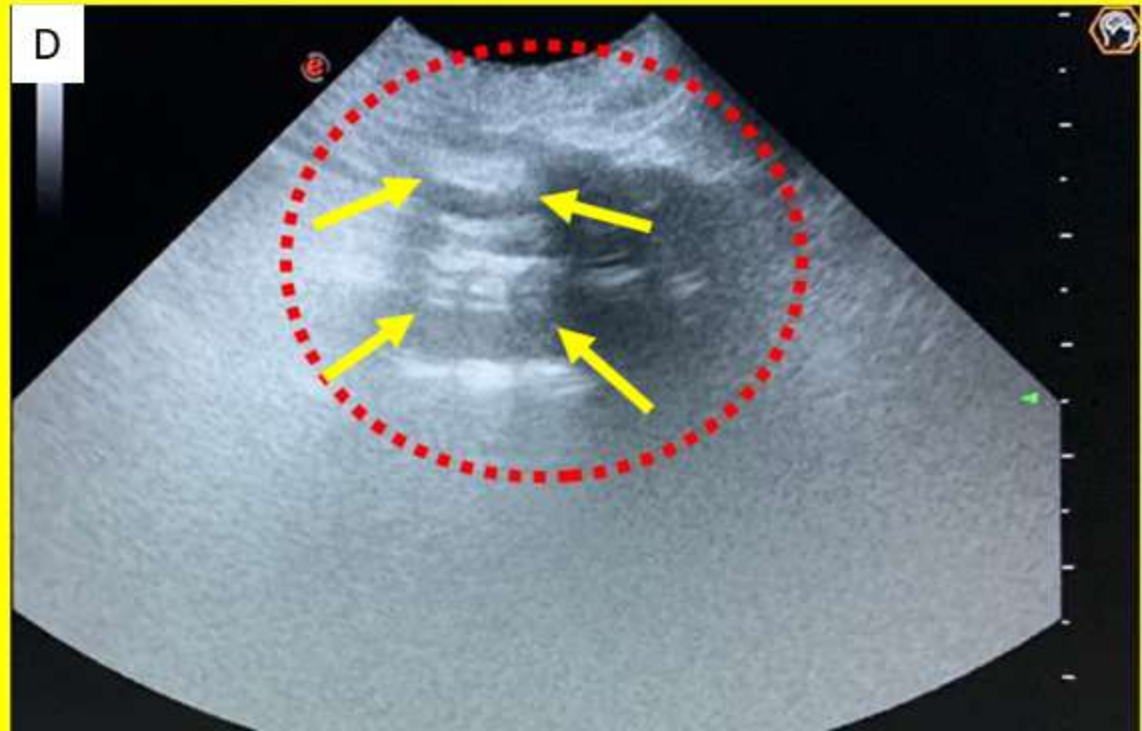


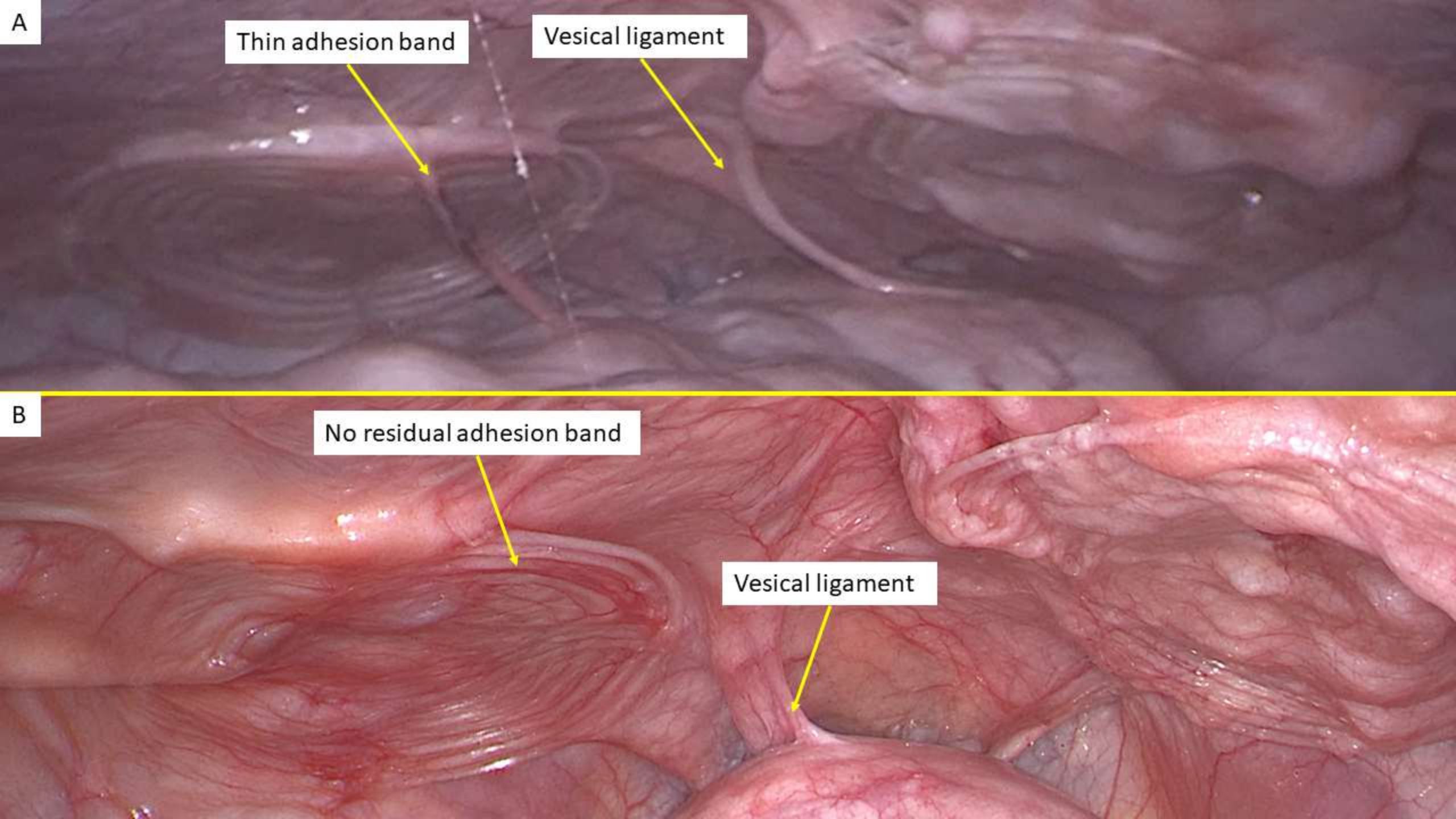
B



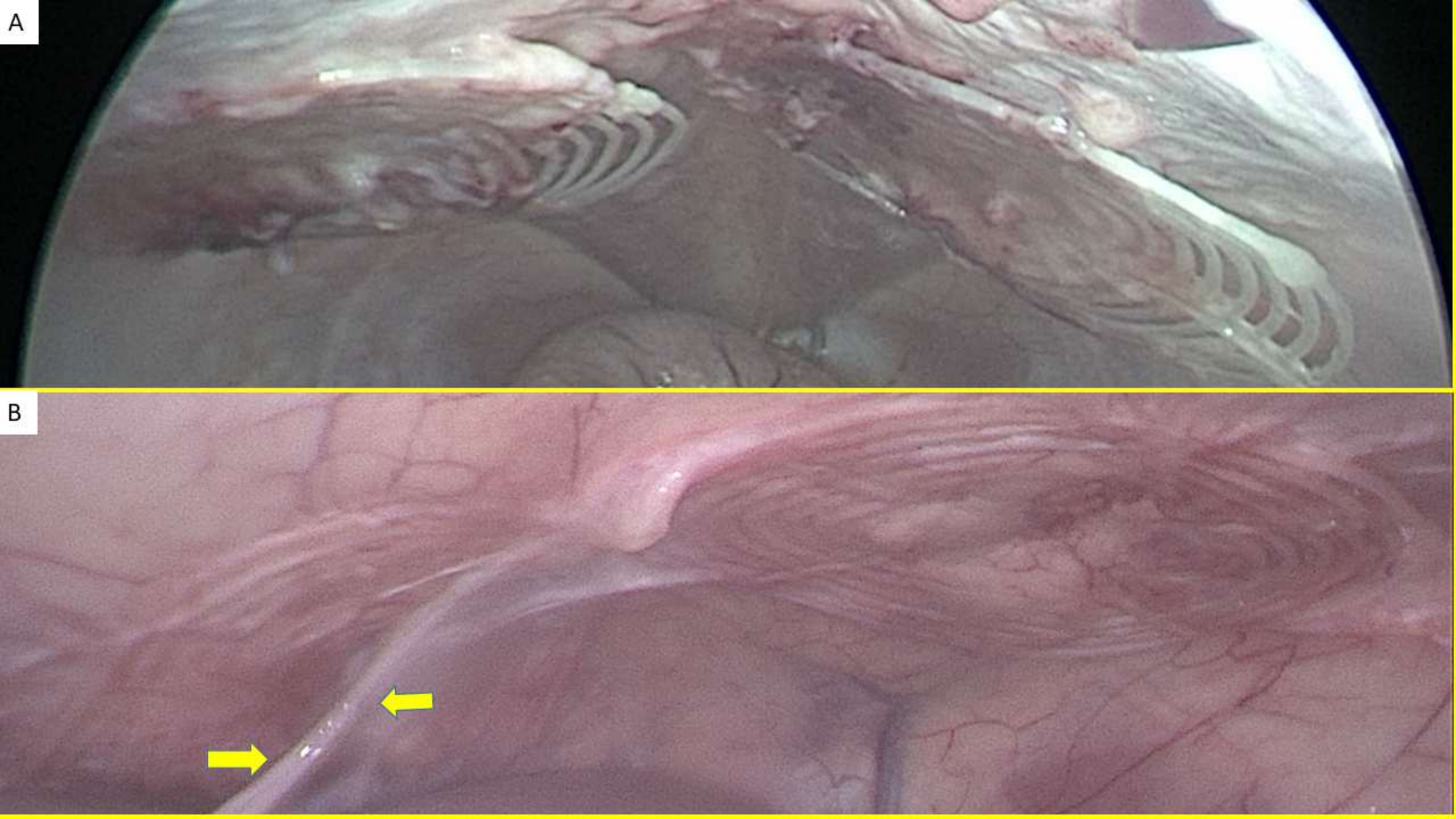


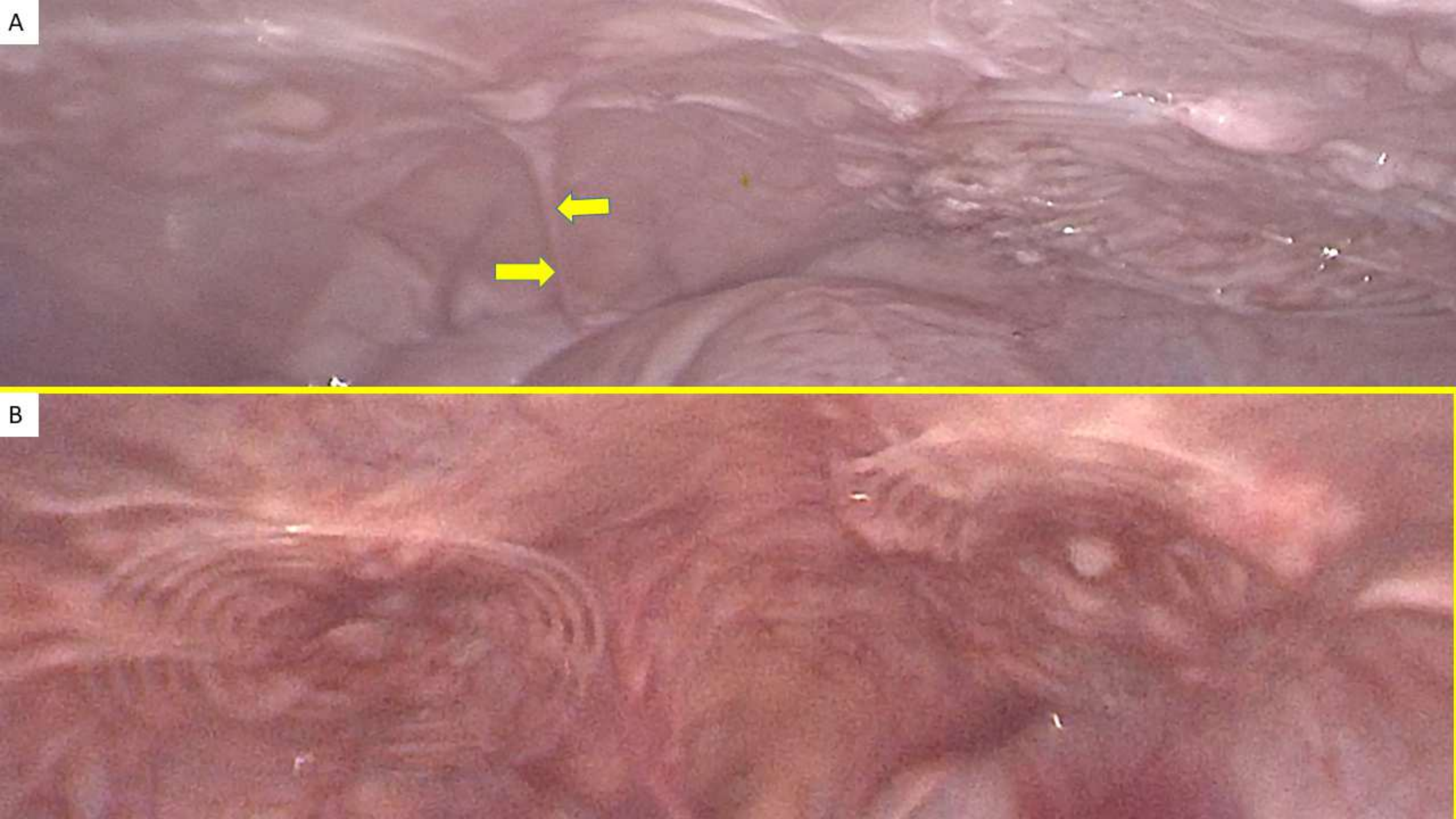
D

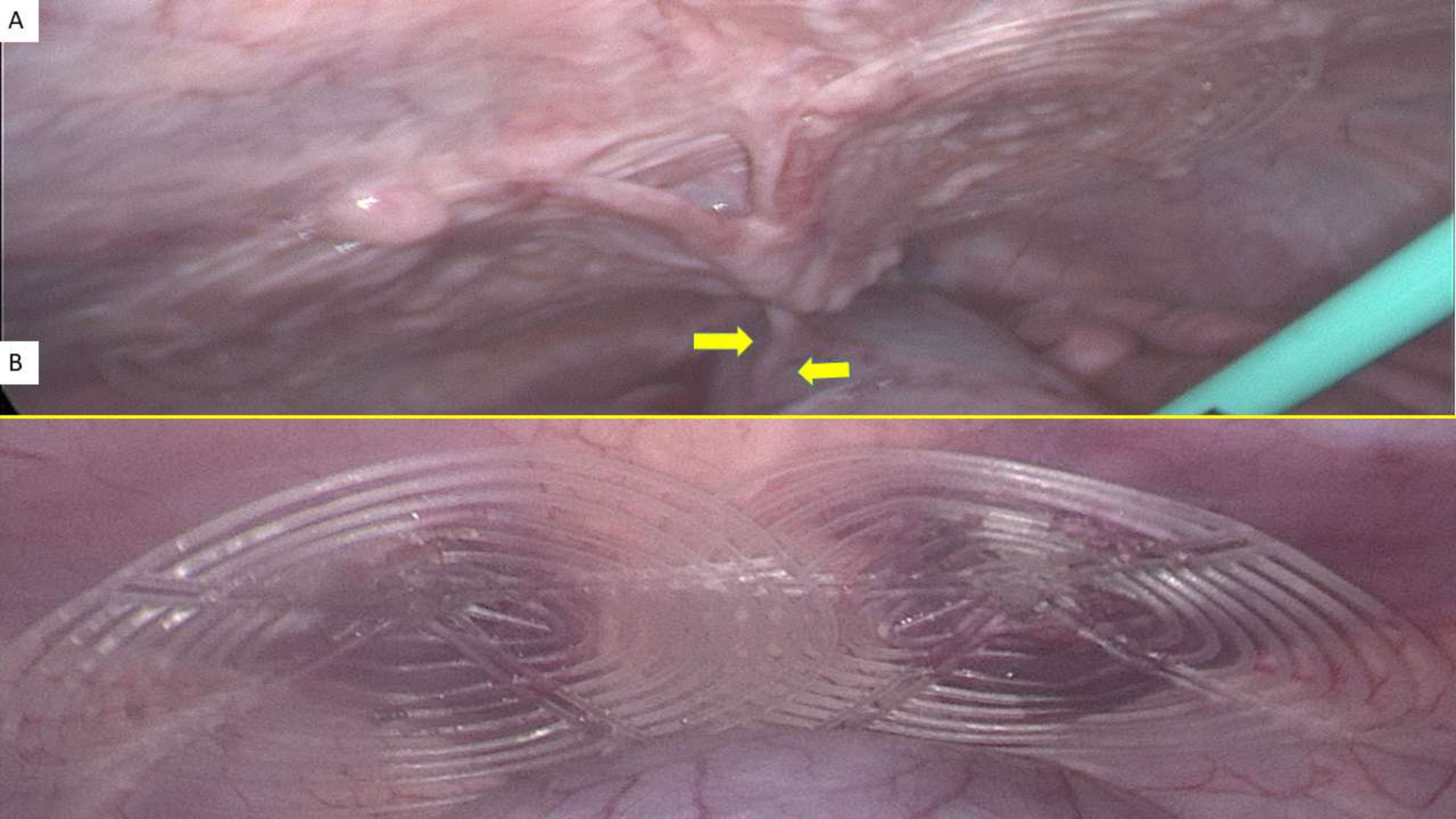


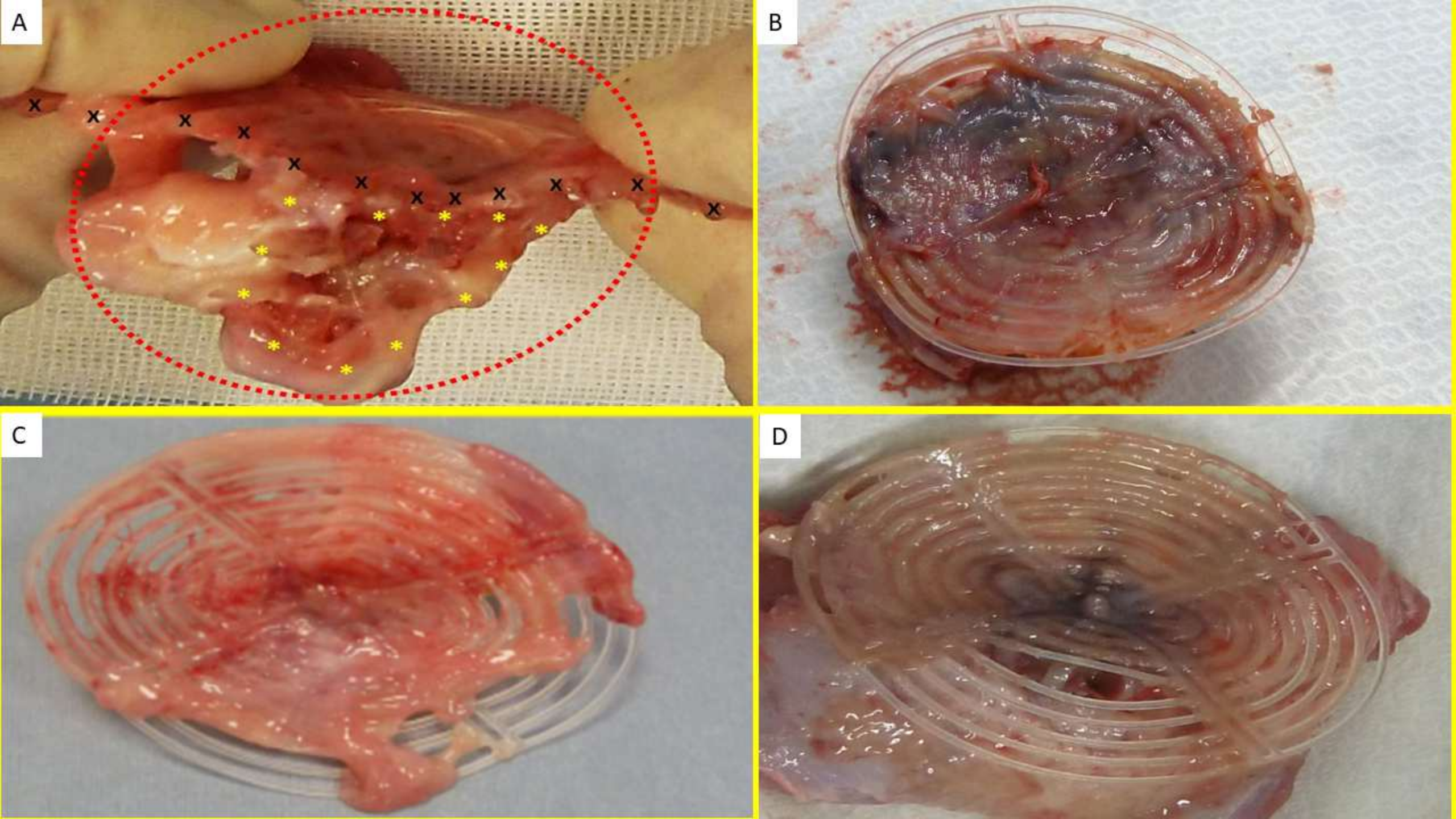

A
Thin adhesion band
Vesical ligament
B
No residual adhesion band
Vesical ligament

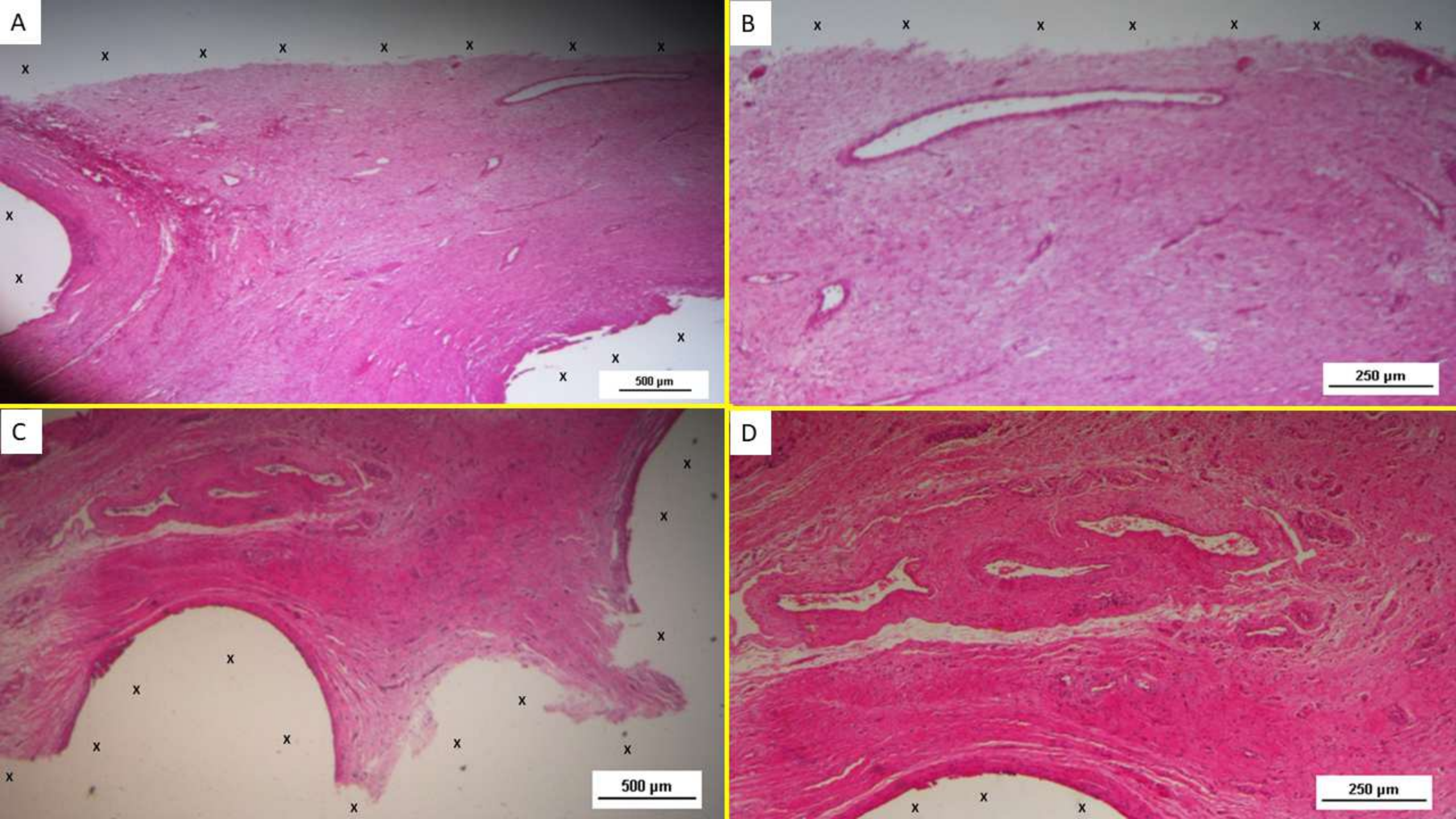

A
B

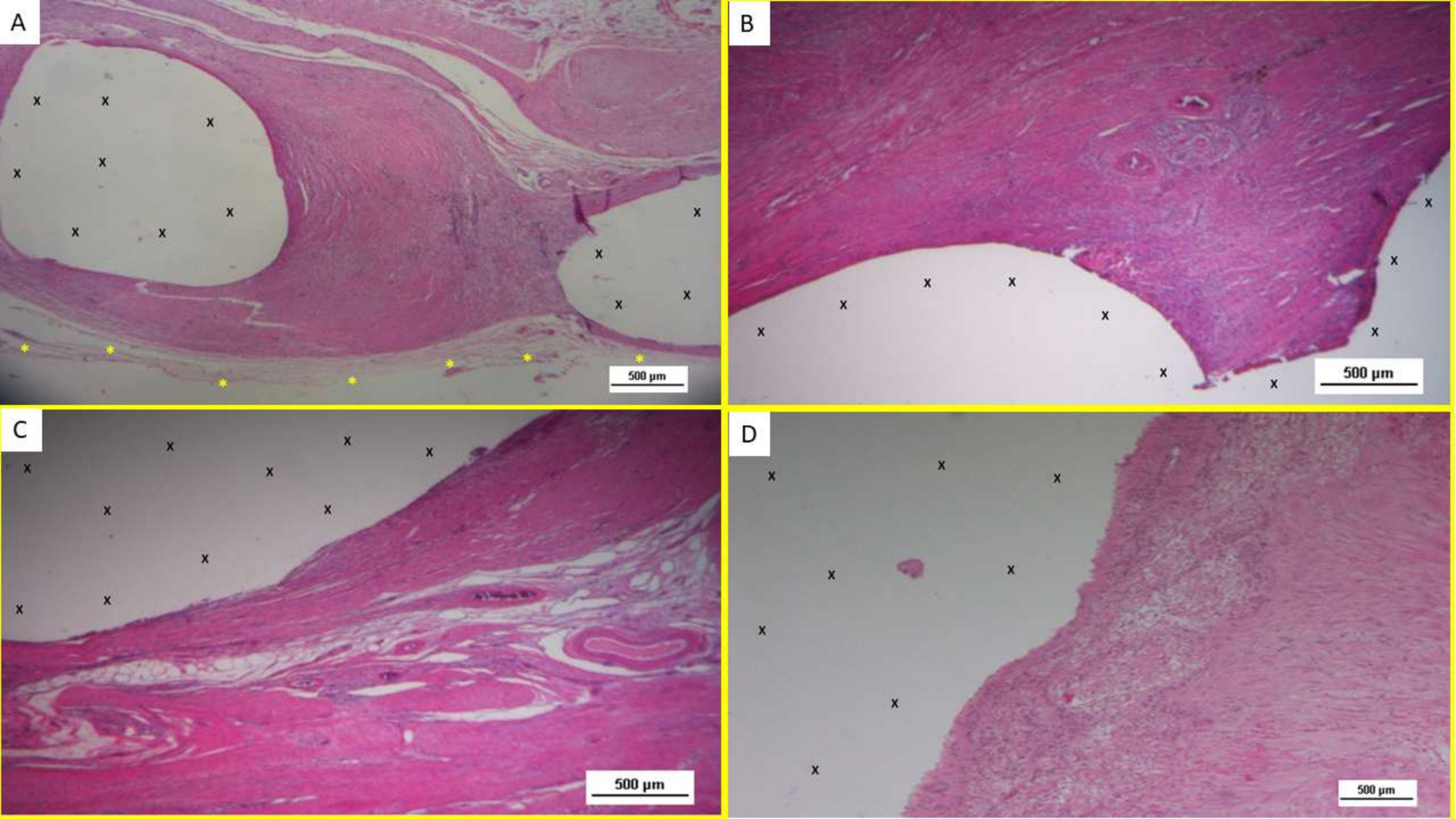

A
B

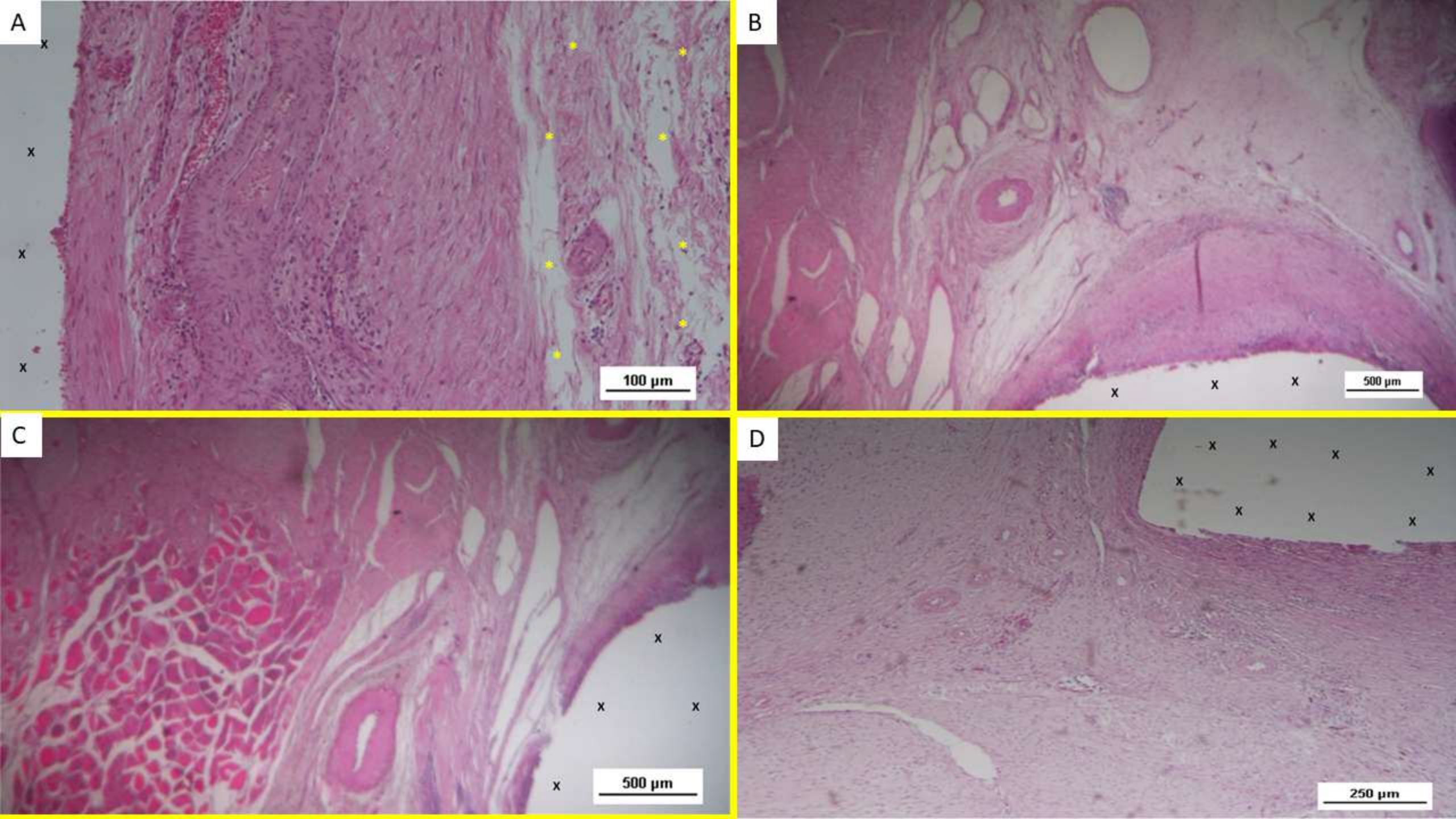

A
B

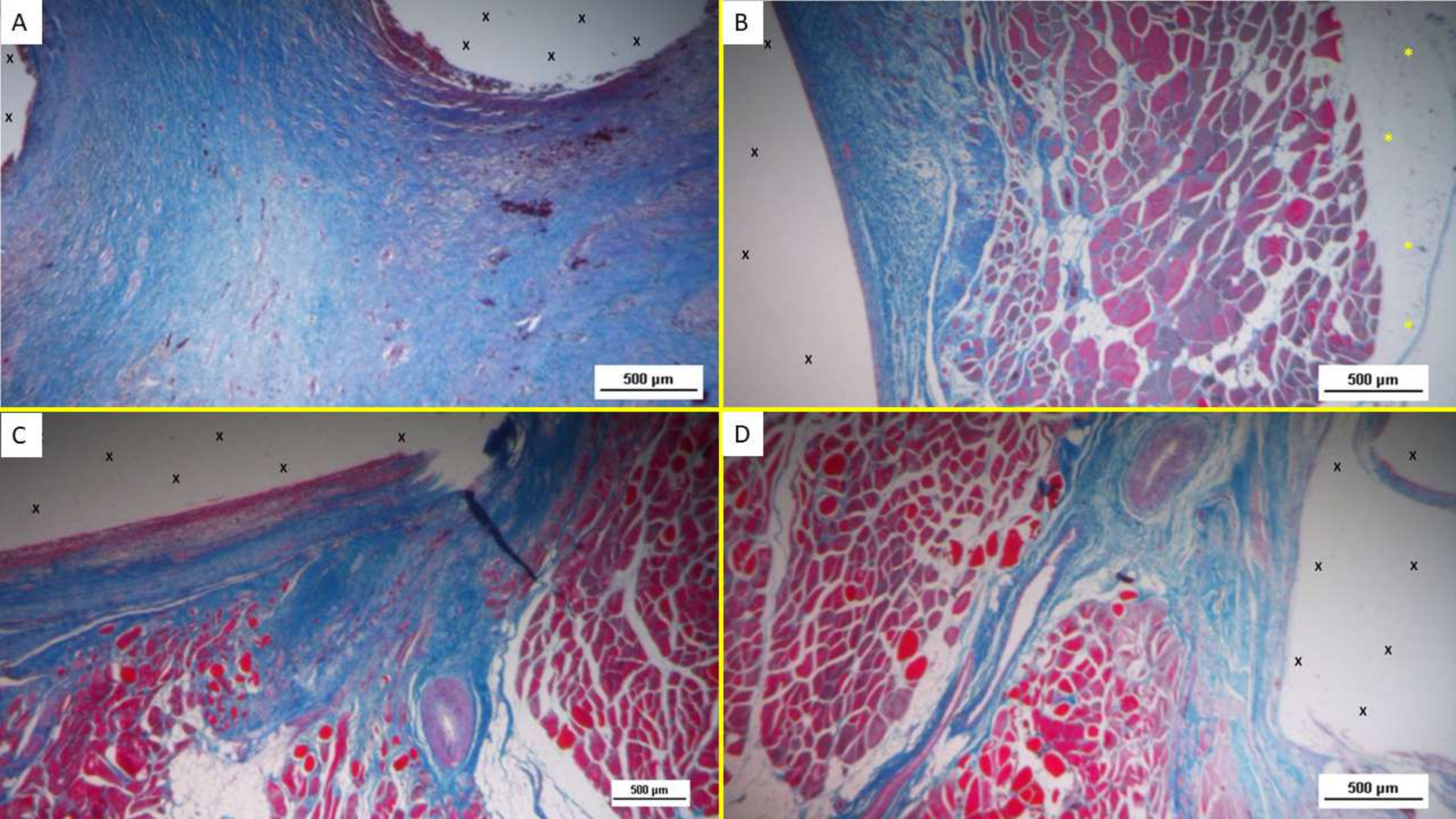

A
B

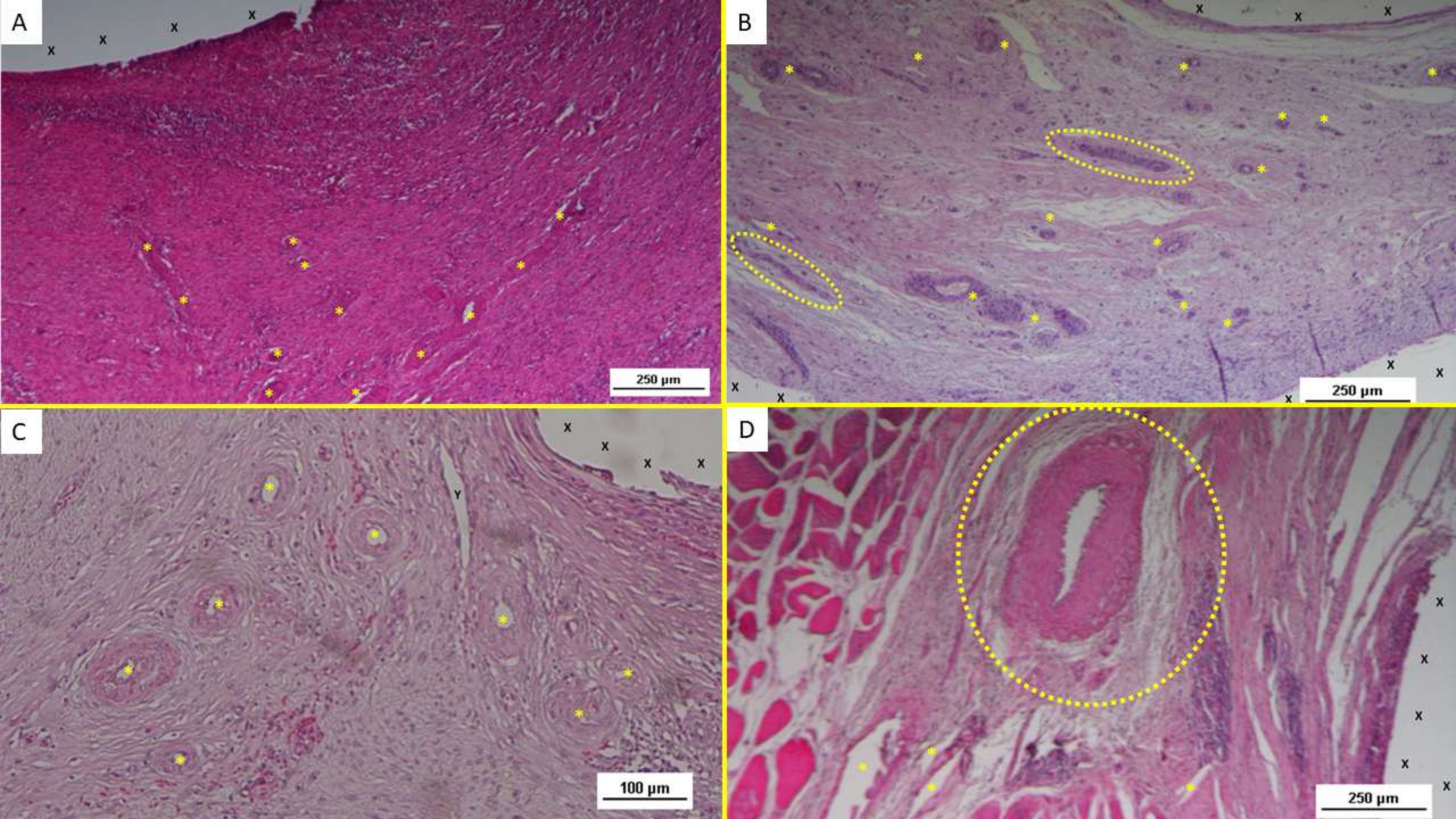

A
B
C
D


A
500 µm
B
250 µm
C
500 µm
D
250 µm


A
500 µm
B
500 µm
C
500 µm
D
500 µm


A
100 µm
B
500 µm
C
500 µm
D
250 µm


A
500 µm
B
500 µm
C
500 µm
D
500 µm


A
250 µm
B
250 µm
C
100 µm
D
250 µm

Supplementary Files

This is a list of supplementary files associated with this preprint. Click to download.

- ArriveChecklistFull.pdf